Iraqi Journal of Physics, 2022 *Vol.20, No. 2, PP.11-25*
DOI: 10.30723/ijp.v20i2.985 *P-ISSN: 2070-4003*
E-ISSN: 2664-5548

Effects of Hydrogen Peroxide Concentration on Properties of Black Silicon Fabricated by Two-Step Silver-Assisted Wet Chemical Etching for Photovoltaics

Auwal Abdulkadir[1a]*, Mohd Zamir Pakhuruddin[2,3b]
[1]Department of Physics, Umaru Musa Yar'adua University, P. M. B. 2218 Katsina, Nigeria
[2]Photovoltaic Materials and Devices, School of Physics, Universiti Sains Malaysia, 11800 Minden, Penang, Malaysia
[3]Institute of Nano Optoelectronics Research and Technology, Universiti Sains Malaysia, 11800 Penang, Malaysia
[b]E-mail: zamir@usm.my
[a]*Corresponding author: auwal.abdulkadir@umyu.edu.ng

Abstract

Crystalline silicon (c-Si) has low optical absorption due to its high surface reflection of incident light. Nanotexturing of c-Si which produces black silicon (b-Si) offers a promising solution. In this work, effect of H_2O_2 concentrations towards surface morphological and optical properties of b-Si fabricated by two-step silver-assisted wet chemical etching (Ag-based two-step MACE) for potential photovoltaic (PV) applications is presented. The method involves a 30 s deposition of silver nanoparticles (Ag NPs) in an aqueous solution of $AgNO_3$:HF (5:6) and an optimized etching in HF:H_2O_2:DI H_2O solution under 0.62 M, 1.85 M, 2.47 M, and 3.7 M concentrations of H_2O_2 at 5 M HF. On the b-Si, nanowires with 250-950 nm heights and an average diameter of 150-280 nm are obtained. Low concentrations of H_2O_2 result in denser nanowires with an average length of 900-950 nm and diameters of about 150-190 nm. The b-Si exhibit outstanding broadband antireflection due to the refractive index grading effect represented as WAR within the 300-1100 nm wavelength region. B-Si obtained after etching in a solution with 0.62 M concentration of H_2O_2, demonstrate WAR of 7.5%. WAR of 7.5% results in an absorption of up to 95.5 % at a wavelength of 600 nm. The enhanced broadband light absorption yields maximum potential short-circuit current density ($J_{sc(max)}$) of up to 38.2 mA/cm^2, or 45.2% enhancement compared to the planar c-Si reference.

Article Info.

Keywords:
Silver-assisted etching, H_2O_2 concentrations, absorption, black silicon, Antireflection.

Article history:
Received: Mar. 05, 2022
Accepted: Apr. 18, 2022
Published: Jun. 01,2022

1. Introduction

Crystalline silicon (c-Si) wafers remain the most attractive absorber materials in the photovoltaic (PV) solar cell manufacturing industries. This is owing to an unceasing development in wafer superiority, maturity of technologies in microelectronics engineering and continuous reduction in wafer cost [1]. However, because of its low absorption coefficient and its indirect bandgap solar cells suffer from poor absorption of light photons. Also, the c-Si's optical absorption is restricted by high surface reflection of about 40% [2]. The high surface reflection loss presents

low light absorption around 300-1100 nm wavelength region within the c-Si absorbers. Low light absorption will always translate to low short-circuit current $J_{sc(max)}$ of the solar cells [2, 3]. Therefore, to ensure maximum achievable $J_{sc(max)}$ of the solar cells (of about 43 mA/cm^2), minimizing optical losses from surface reflection for enhanced optical absorption in the c-Si is necessary.

Fabrication of nanotextures on c-Si wafers to produce nanopores, nano walls, nano spikes, or nanowires with dimensions smaller than the incident light's wavelength (called "black silicon" (b-Si)) is a facile method to diminish the high surface reflection of the c-Si wafers [4-6]. With b-Si, it is possible to reduce c-Si's surface reflection to less than 10% within 300-1100 nm wavelength region [4-6]. Metal-assisted wet chemical etching (MACE) and reactive-ion-etching (RIE) processes are the most convenient approaches reported in the literature to realize such nanotextures on c-Si [7]. One-step or two-step silver-assisted MACE (Ag-based MACE), which comprises Ag nanoparticles (NPs) catalysts nucleation and random etching, is the most appealing approach due to its facile and low-cost nature compared to RIE [8]. In one-step Ag-based MACE, the Ag NPs catalysts nucleation and random etching takes place concurrently in $AgNO_3$:HF aqueous solution [7-9]. However, nanopores, nano walls, nano spikes or nanowires produced via one-step Ag-based MACE possess a typical height of around 1-10 µm. Such lengthy nanotextures demonstrate high recombination of electrons and holes charge carriers in the b-Si solar cells [9-11]. Two-step Ag-based MACE involves short time dip in $AgNO_3$:HF aqueous solution to separately deposit the Ag NPs catalyst on c-Si and a successive etching in HF:H_2O_2 solution to produce nanopores, nano walls, nano spikes, or nanowires with less than 1 µm depth of pores or heights [11, 12]. Thus, the two-step Ag-based MACE is an interesting method to fabricate the nanopores, nano walls, nano spikes, or nanowires with heights of less than 1 µm for low carrier recombination-based efficient b-Si solar cells [12, 13]. Li et al. reported a two-step Ag-based MACE fabrication method of producing nanopore type b-Si with nanopores depth ranges of 318-886 nm on p-type c-Si wafers having (200 ± 20 µm thick with 1–3 Ω cm resistivity) for broadband antireflection and application in b-Si solar cells [14]. In their work, the Ag NPs catalyst deposition was achieved by dipping the wafers in a solution of $AgNO_3$:HF. Successive etching of the Ag NPs catalyst deposited wafer was done in a solution containing HF:H_2O_2:DI H_2O for few minutes. Recently, Bahera et al. reported a two-step Ag-based MACE process for fabrication of b-Si nano walls on p-type (boron-doped), one polished side c-Si (100) wafers with a resistivity of 1–10 Ω.cm to demonstrates broadband antireflection for applications in b-Si solar cells [15]. In their work, Ag NPs catalyst was deposited on polished c-Si surface by exposing it to a solution consisting of HF and $AgNO_3$ (5% HF + 0.02 M $AgNO_3$) for different deposition times of 15, 30, 45 and 60 s. From their analysis, 60 s deposition time was the optimum to produce stable b-Si nano walls with uniform wall thickness. After etching the 60 s Ag NPs catalyst deposited c-Si wafer in a solution of 4.8 M HF and 0.2 M H_2O_2, b-Si with nano walls of an average thickness of ~60 nm was realized. The nano walls suppress surface reflection of the wafer to the best of ~1.5% over 280-1107 wavelength region. Besides, Chaves et al. reported studies on morphological properties of b-Si nanowires fabricated on p-type (100) c-Si wafer with a resistivity of 1–10 Ωcm via two-step Ag-based MACE [16]. In their studies, the nanowires' formation dependence on Ag NPs catalyst deposition time (in 88 mM $AgNO_3$:5% HF) between 10-20 s and etching time (in 3% HF:10% H_2O_2) between 30-45 min was investigated for potential applications in b-Si solar cells. To the best of our knowledge, numerous studies have been carried out to examine the antireflection

and morphological properties of lightly (boron) doped c-Si (100) wafers at room temperature. However, the literature works are centered only on the effect of etching and deposition time on the morphological and optical properties of the b-Si wafers. Thus, there are limited studies on the effect of H_2O_2 concentration on the morphological and optical properties for an enhanced optical absorption of the c-Si wafers within 300-1100 nm wavelength region. Available studies presented in the literature by Li et. al. and Liu et. al. on the effect of H_2O_2 concentrations on b-Si formation are only geared towards the correlation between the H_2O_2 concentrations, length of the nanowires and their impact on the weight average reflection (WAR) [17, 18]. Generally, the WAR is not governed by the height of the nanowires only. The surface coverage and base diameters of the nanowires are other important parameters which determine the efficacy of refractive index grading effect for lower WAR. This justifies the need for further investigations into the effect of H_2O_2 concentrations towards the surface coverage and base diameters of the nanowires over the c-Si wafer surface.

This paper presents an investigation on the effect of H_2O_2 concentrations on b-Si formation for potential applications in solar cells. The method adopted is based on a two-step Ag-based MACE process comprising a short time duration for the Ag NPs catalyst deposition in $AgNO_3$:HF and a successive etching in solutions of HF:H_2O_2 having different H_2O_2 concentrations. Morphological and optical properties of the b-Si produced with H_2O_2 of different concentrations are then analyzed. Using the enhanced optical absorption data, achievable $J_{sc(max)}$ was calculated to comparatively attest light-trapping capability of the b-Si fabricated with different H_2O_2 concentrations across the 300-1100 nm wavelength region. From this work, a correlation between H_2O_2 concentration, b-Si nanowires' length, b-Si nanowires' diameter, WAR and $J_{sc(max)}$ has been established.

2. Materials and methods

P-type (boron-doped, 1–10 Ω.cm resistivity) 250 μm-thick c-Si wafers with (100) orientations are used as the starting substrates. To clean the wafers and remove oxide layer, organic residues, and metallic contaminants, Radio Corporation of America (RCA) cleaning process was adopted [19]. For the b-Si fabrication process, H_2O_2 (30%), HF (49%) and, $AgNO_3$ (2.5% w/v in H_2O), were employed. For Ag NPs catalyst deposition, the c-Si wafers were placed in a solution of 5:6 ($AgNO_3$:HF) at room temperature for 30 s. Successive optimized etching in a solution of HF:H_2O_2:DI H_2O was then performed to produce the b-Si as reported in our previous works [12, 20, 21]. The etching was conducted under different concentrations of H_2O_2 at a constant concentration of HF as presented in Table 1. The wafers were leveled as W (i.e. 0.62 M), X (i.e. 1.85 M), Y (i.e. 2.47 M) and Z (i.e. 3.7 M) after the etching according to the concentrations of H_2O_2.

Results of b-Si realized with optimized 1.23 M concentration of H_2O_2 can be seen in our previous publications [20, 21].

Table 1: Two-step MACE process with different H_2O_2 concentrations.

H_2O_2 concentration (M)	**Volume ratio of HF:H_2O_2:H_2O**	**HF concentration (M)**
W: 0.62 M	4:1:11	7.04
X: 1.85 M	4:3:9	7.04
Y: 2.47 M	4:4:8	7.04
Z: 3.70 M	4:6:6	7.04

After the two-step Ag-based MACE etching process, residual Ag NPs catalyst on c-Si, was detached using un-diluted HNO_3 (60%). Before N_2 drying, the thin SiO_2 layer grown during the detachment of residual Ag NPs catalyst, was removed using dip in a solution of 5% HF for 60 s. Field Emission Scanning Electron Microscopy (FESEM) (model: FEI Nova NanoSEM 450) was used to characterized top view, tilted angle (30^o) and cross-section of the fabricated b-Si. Hemispherical reflection of the b-Si samples etched with different concentrations of H_2O_2 was measured by Cary 5000 UV-VIS-NIR spectrophotometer equipped with an integrating sphere, hemispherical reflection over 300-1100 nm wavelength region were measured. Light coupling performance of the fabricated b-Si samples was evaluated using WAR %. The WAR was calculated by integrating the surface reflection of the b-Si with AM1.5 global solar spectrum over 300-1100 nm wavelength region. This is expressed in Eq.(1) [3, 22], where R(λ) is the reflection, and S(λ) denotes the AM1.5 global solar spectrum.

$$WAR(\lambda) = \frac{\int_{300\ nm}^{1100\ nm} \boldsymbol{R(\lambda)S(\lambda)d\lambda}}{\int_{300\ nm}^{1100\ nm} \boldsymbol{S(\lambda)d\lambda}} \quad \textbf{(1)}$$

Absorption (A = 100−R−T %) was calculated using the hemispherical reflection data. This was done with the assumption that, Transmission (T) is zero for an opaque c-Si wafer. The property of an opaque material was characterized with absorption and reflection of incident light while transmission of light at the other end is believed to be negligible [22]. Using the optical absorption data, potential $J_{sc(max)}$ was theoretically estimated using Eq.(2). In Eq.(2), S(ʎ) is the standard spectral photon density of sunlight for the AM1.5 global solar spectrum and q is the electron charge [22]. During the calculations using Equation (2), unity internal quantum efficiency; IQE=1, was assumed for the b-Si samples and planar c-Si reference. From the calculated $J_{sc(max)}$, $J_{sc(max)}$ normalization between b-Si samples and reference c-Si was done to realize the enhancement in the potential $J_{sc(max)}$. This is an important figure of merits (FOM) to visualize the effect of H_2O_2 concentration on length of nanowires, average diameters, WAR, and its impacts on potential $J_{sc(max)}$ enhancement.

$$J_{sc(max)} = q \int_{300\ nm}^{1100\ nm} EQE(\lambda).S(\lambda)\, d\lambda \quad \textbf{(2)}$$

3. Results and discussion

B-Si formation mechanism in the two-step Ag-based MACE involves formation of self-assembled electrochemical cells with reduction, anodic, and cathodic reactions described by Eqs. ((3)-(10)). Initially when c-Si is dipped in a solution of $AgNO_3$:HF, Ag^+ ions are reduced to Ag nuclei owing to electrons capture from the contacted c-Si's valence band. Electron capturing happens because Ag is more electronegative than c-Si. Formation of HNO_3 through a reaction between H^+ and $(NO_3)^-$ ions and the Ag reduction process are defined by Eq. (3)-(6) [11, 23-25]. After dipping the Ag NPs catalyst deposited wafer in a solution of HF:H_2O_2:DI H_2O, the regions of the c-Si surface that are already contacted with Ag NPs catalyst get oxidized and later the SiO_2 is removed by the HF. The process leaves vertically oriented nanowires on the c-Si in a $H_2SiF_6 + 2H_2O$ final solution (Eq. ((7)-(8)) [11, 23-25].
The reduction reaction during Ag NPs deposition (in $AgNO_3$:HF) is:

$$AgNO_3 \rightarrow \quad Ag^+ + (NO_3)^- \quad \textbf{(3)}$$

$$Ag^+ + e^- \rightarrow Ag^o(s) \quad \textbf{(4)}$$

$$HF \rightarrow F^- + H^+ \quad \textbf{(5)}$$

$$H^+ + (NO_3)^- \rightarrow HNO_3 \quad \textbf{(6)}$$

The anodic reaction (occurring at the contact point between the c-Si and the Ag NPs) is:

$$Si(s) + 2H_2O \rightarrow SiO_2 + 4H^+ + 4e^- \quad \textbf{(7)}$$

$$SiO_2(s) + 6HF \rightarrow H_2SiF_6 + 2H_2O \quad \textbf{(8)}$$

The cathodic reaction (at the Ag NPs surface) is:

$$H_2O_2 + 2H^+ \rightarrow 2H_2O + 2h^+ \quad \textbf{(9)}$$

$$2H+ \rightarrow H_2 \uparrow + 2h^+ \quad \textbf{(10)}$$

The cathodic process taking place at the Ag NPs catalyst surface during the etching in HF:H_2O_2:DI H_2O is described by Eqs. (9 and 10). Eqs. (9 and 10) indicate holes injection into the valence band of c-Si causing H_2O_2 reduction during the etching process. Meaning, when the Ag NPs deposited wafers are dipped in a solution of HF:H_2O_2:DI H_2O, the regions of the c-Si surface that are already contacted with the Ag NPs catalyst get oxidized by the H_2O_2 owing to the high reduction potential (E^o (v); 1.8 V) of H_2O_2 compared to that of c-Si bulk [24]. As the process is prolonged, the SiO_2 then get removed by the HF. Thus, since c-Si surface that is in contact with the Ag NPs catalyst becomes oxidized by the H_2O_2 oxidant with the liberation of hydrogen while the HF removal of SiO_2 proceeds, then the concentration of H_2O_2 will determine the rate of hydrogen liberation as well as the etching rate and the etching direction.

Fig. 1 presents top view and 30^o tilted FESEM images of the b-Si samples produced after etching with different H_2O_2 concentrations. The figure illustrated that b-Si surfaces produced after etching with different H_2O_2 concentrations compose nanowires with different sizes over the c-Si wafer. For samples W and X (Fig. 1 ((a) and (b), (c) and (d)), the surface of the samples is covered with dense and finely formed nanowires. However, a slight increase in interspacing between nanowires is observed for the sample X (Fig. 1 (d)). The increased interspacing may represent a slight increase in the mean average base diameters of the nanowires. For sample Y, slight shrinking of the nanowires' heights is observed in some areas (balding) as observed from Fig. 1 (e and f). Shrinking of nanowires over the c-Si wafer surface is observed to increase further after etching with 3.7 M concentration of H_2O_2 as illustrated by Fig. 1 (g) and (h) (sample Z).

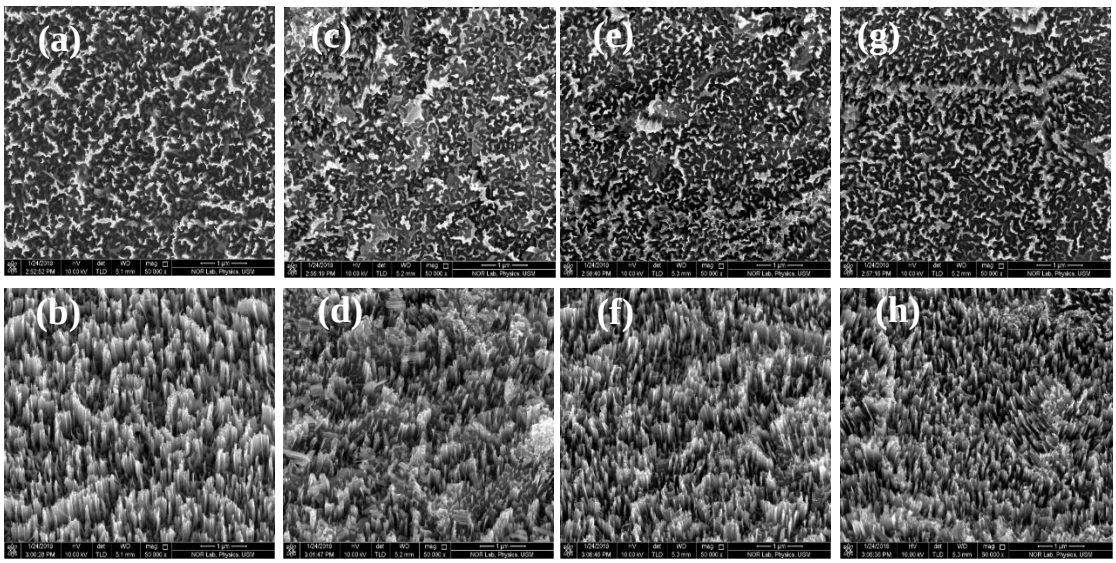

Figure 1: Top view and 30^o oblique FESEM images of b-Si etched with different H_2O_2 concentrations; ((a) and (b)) W: 0.62 M ((c) and (d)) X: 1.85 M ((e) and (f)) Y: 2.47 M ((g) and (h)) Z: 3.7 M. The scale bar is with 1 µm length.

Fig. 2 illustrates the cross-sectional FESEM images of W, X, Y, and Z b-Si samples fabricated with different concentrations of H_2O_2. In consistence with the top sight and 30^o tilted FESEM images of the b-Si samples shown in Fig. 1, Fig. 2 shows that the nanowires are characterized by a dissimilar average height and mean average diameters. For samples W and X, the nanowires possess a mean average height of 900 nm and 950.5 nm. Sample W has a mean average diameter of about 150 nm and sample X has 190 nm. The possession of a slightly higher mean average diameter by sample X is expected. This owes to the slight increase in the interspacing between nanowires as observed earlier for the sample (refer to Fig. 1 (d)). The mechanism of the slight increase in the interspacing among the nanowires lies in the lateral etching favored by the higher concentration of H_2O_2 (refer to Fig. 3). A slight increase in length from 900 nm to 950 nm and mean average diameter from 150 nm to 190 nm for the sample etched with 1.85 M H_2O_2 is due to the increased H_2O_2 concentration, which acts as a hole donor as well as an oxidant agent in the etching process (refer to Eqs. (9) and (10)). This increases the oxidation speed of the c-Si around the Ag NPs, thus, resulting in an increase in both the horizontal and vertical etching speeds [19].

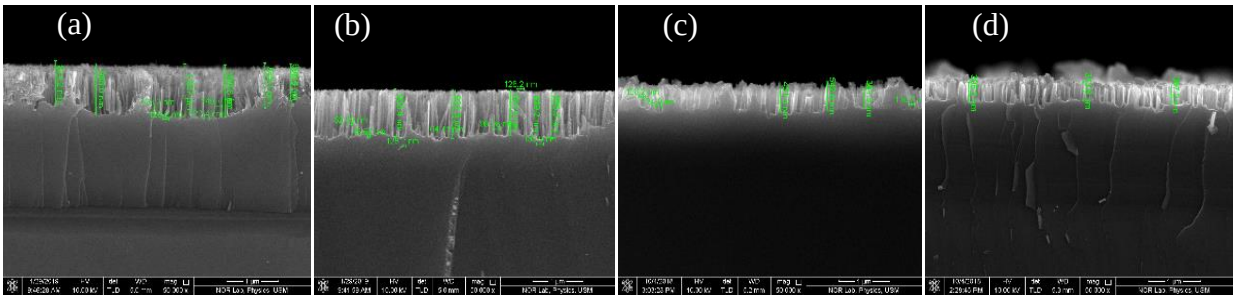

Figure 2: Cross-sectional FESEM images of b-Si nanowires etched with different H_2O_2 concentrations; (a) W: 0.62 M (b) X: 1.85 (c) Y: 2.47 M (d) Z: 3.7 M. The scale bar is with 1 µm length.

For sample Y, etched with 2.47 M H_2O_2, the nanowires' heights were reduced to 650.0 nm. After using H_2O_2 concentrations of 3.7 M during the etching process

(sample Z), the nanowires' length decreased to the minimum level of around 350-200 nm (with an average value of 250 nm) due to the presence of a low concentration of HF, which facilitates the SiO_2 removal. The nanowires' mean average diameters increased to around 250.3 nm, and 280.9 nm (nearly porous) for samples Y and Z, respectively. The realized reduction in nanowires' height owes to increased H_2O_2 concentration that pauses the speedy advancement of the SiO_2 removal by HF during the etching. Slow etching makes the Ag NPs catalyst stay longer on c-Si wafer surfaces, thus triggering lateral etching along Si-Si bond. Lateral etching could yield nanowires with larger mean average diameters in b-Si [17,18]. Besides, in two-step Ag-based MACE the SiO_2 removal depends on the number of holes injected into the c-Si by the H_2O_2 hole donor (refer to Eq.(9) and (10)). Therefore, with low concentration of H_2O_2, hole injection is limited to the (100) plane. C-Si has fewest back bonds to break along (100) plane, due to this the etching only proceeds faster and selectively along the (100) direction. Increasing H_2O_2 concentration, may then cause huge generation of holes that results in excessive and speedy etching of c-Si atoms in other crystals. Etching of c-Si atoms in other crystal planes resulted in etching along (110) and (111) planes, thus producing nanowires with larger mean averaged diameters and smaller lengths [17,18]. The findings are consistent with the observations reported by Li et al. [17] and Liu et al. [18]. Both reported that lengths of nanowires increase with an increase in H_2O_2 concentration up to an optimum point and later shrink to lower lengths with higher concentrations of H_2O_2.

Overall mechanism of the etching process under low and high H_2O_2 concentrations are schematically illustrated in Fig.3. For low H_2O_2 concentrations (samples W and X), the shape of the base diameters for b-Si nanowires appear to be nearly rounded (i.e. circular) with high lengths due to presence of enough HF to disolve the SiO_2 (Fig. 3 (a)) as discussed earlier. Possesion of square-like shape base diameters for samples etched with low H_2O_2 concentration is owing to the faster etching rate due to the presence of a high HF concentration during the etching process. A square-like shape diameter occur due to high available HF which dissolves the SiO_2 under the Ag NPs. The availability of enough HF makes the Ag NPs move faster down to the c-Si bulk thereby yielding nanowires with a high length.

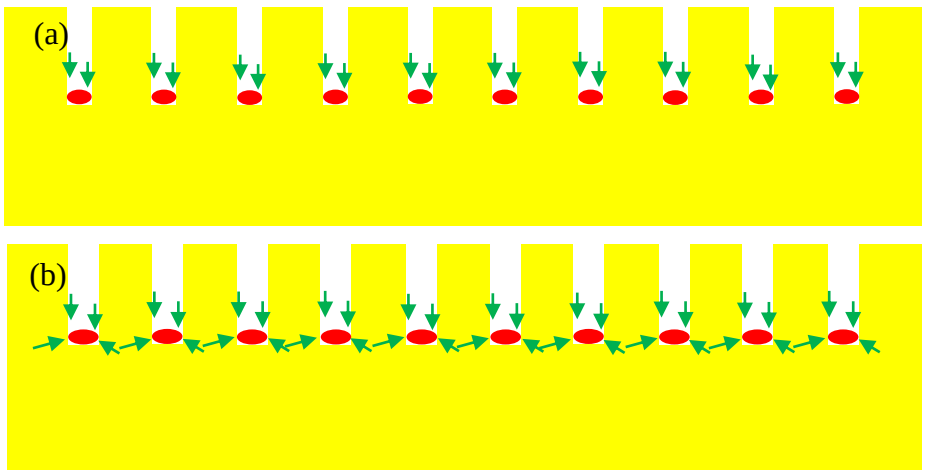

Figure 3: Schematic diagram showing favored etching directions of c-Si: (a) under low H_2O_2 concentration and (b) under high H_2O_2 concentration. The diagram is not drawn to scale.

For samples etched with high concentrations of H_2O_2 (samples Y and Z), grown Ag NPs accumulates new Ag nuclei to become bigger NPs on the c-Si due to low available HF to dissolve the SiO_2 under the Ag NPs during the etching process. When the Ag NPs stay longer on c-Si before the SiO_2 gets etched by the HF, already grown Ag NPs accumulates new Ag ion and becomes heavier on c-Si (Fig. 3 (b)), thus making their shape square at the base contact with c-Si thereby yielding nanowires with shorter length after the etching. Another possible reason could be due to the square Si-Si bonding of a (100) c-Si wafer surface (i.e. the starting substrate), making the obtained outlines of sunk Ag NPs from the chemical etching to consequently be nearly square. Therefore, the realization of square-like diameters is because, with low HF concentration (due to presence of high H_2O_2 concentration), the c-Si etching rate slows down, leading the SiO_2 removal processes prefer to occur faster along the direction of Si-Si bonding for the (100) c-Si wafers as also suggested by other findings [17,18].

Fig. 4 shows the optical reflection and optical absorption profiles of W, X, Y, and Z b-Si samples. The surface reflection of the etched b-Si samples is less than that of the un-etched reference c-Si. Possession of lower surface reflection by the W, X, Y and Z b-Si samples owes to the presence of nanowires on the samples etched with different concentrations of H_2O_2. The b-Si samples reveal lower surface reflection with an enhanced optical absorption across the 300-1100 nm wavelength region. The enhanced absorption is due to the improved light-trapping resulting from the refractive index grading effect at the interface of air and c-Si, due to the existence of the light-trapping nanowires [26]. Incident light on the light-trapping nanowires at the c-Si surface, will perceive the surface as a homogenous medium with refractive index (n) that gradually changes from that of air (n=1) to that of the c-Si (n=3.8). This results in the reduction of the surface reflection from the c-Si surface and enhances optical absorption across the 300-1100 nm wavelength range [26, 27]. Overall, not many changes were observed in terms of the surface reflection reduction among the samples etched with different H_2O_2 concentrations. The reason is because all samples are characterized with nanowires having an average height of greater than 250 nm which is the minimum height for effective refractive index grading as reported in the literature [28, 29]. Besides, beyond the 800 nm region, all the W, X, Y, and Z b-Si samples show steady rise to higher values of surface reflection. The gradual increase in the surface reflection is higher for samples etched with 2.47 M and 3.70 M H_2O_2. This may arise due to surface balding and b-Si nanowires shrinking for samples etched with higher concentrations of H_2O_2 (refer to Fig.1 (f) and (h)) which may affect the refractive index grading effect when light traverses from air to c-Si. WAR values of 7.5 %, 9.1%, 10.6% and 11.1% were obtained for the W, X, Y, and Z b-Si samples, respectively.

The W, X, Y, and Z b-Si samples have the same optical absorptions of 95.5%, 94.5%, 93.4%, and 92.2%, respectively at 600 nm wavelength region. The increase in WAR observed for sample X irrespective of having lengthy nanowires compared to sample W, is due to possession of slightly higher average base diameters by sample etched with 1.85 M H_2O_2 (sample X). The increased average diameter is due to the slight increase in the interspacing between the b-Si nanowires, as earlier illustrated in Fig. 1 (d) and 2 (b). Realization of high WAR values for samples etched with 2.47 M and 3.7 M H_2O_2 (samples Y and Z) is ascribed to the increase in the nanowires mean average diameters to an averaged value of around 250.3 nm and 280.9 nm (nearly porous), respectively.

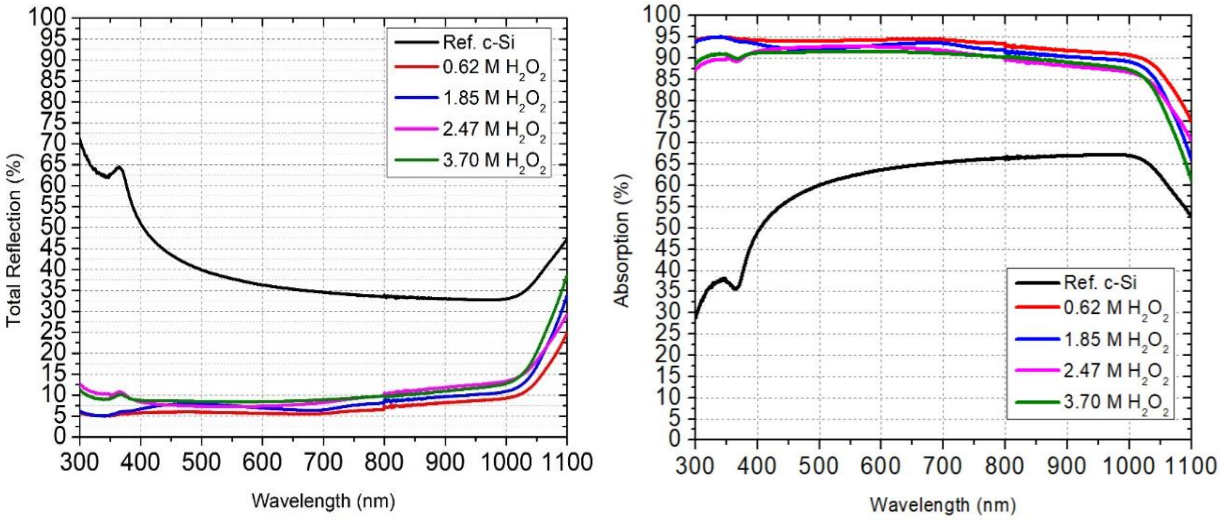

(a) (b)

Figure 4: (a) Reflection curves (b) Absorption curves of b-Si nanowires etched with different H_2O_2 concentrations; W: 0.62 M, X: 1.85 M, Y: 2.47 M, Z: 3.70 M.

This work reveals that, for the realization of good light trapping b-Si for efficient solar cells, lower H_2O_2 concentration (between 0.60 M-2.0M) is optimum during the Ag-based two-step MACE process as also reported by other works [19, 28]. Higher concentrations of H_2O_2 tend to enlarge the base diameters of the produced nanowires, which cause an increased reflection that consequently translates to low optical absorption irrespective of the nanowires' lengths.

The relationship between H_2O_2 concentration, the length, mean average diameter of the nanowires, and WAR are presented in Fig.5. Consistent with the literature, Fig. 5 (a) reveals that the length of nanowires increases with an increase in the H_2O_2 concentration up to a maximum H_2O_2 concentration of about ~2.0 M after which the height of nanowires decreases to lower values at H_2O_2 concentrations of 2.47 M and 3.7 M [17, 18]. However, the lowest WAR (7.5%) was realized for the sample etched with H_2O_2 of 0.62 M concentration (sample W) despite having shorter nanowires of around 900 nm compared to sample X etched with 1.85 M H_2O_2 (nanowires of 950.5 nm). From Fig.5 (b), it is observed that the average diameters of nanowires increase with increasing H_2O_2 concentration. The increase in diameter from 150 nm to 190 nm, 250.3 nm, and 280.9 nm causes an increase in WAR of the b-Si from 7.5 % to 9.1%, 10.6%, and 11.1% for samples W, X, Y, and Z etched with H_2O_2 of 0.62 M, 1.87 M, 2.47 M, and 3.7 M concentrations, respectively.

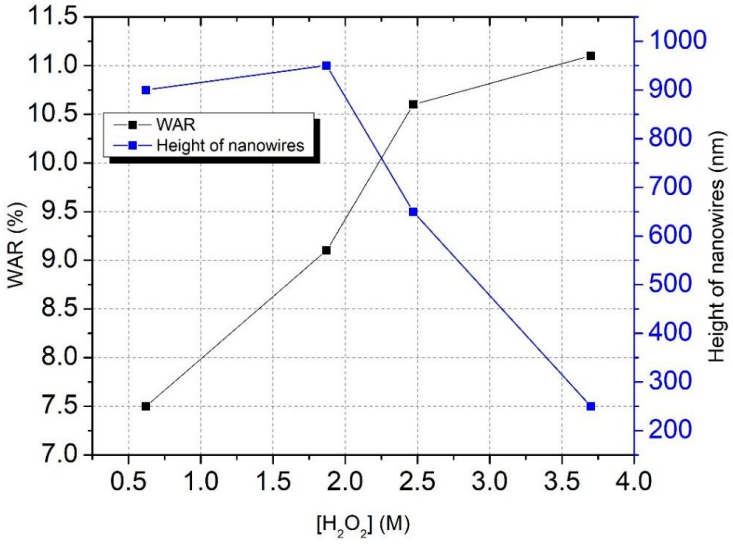

(a)

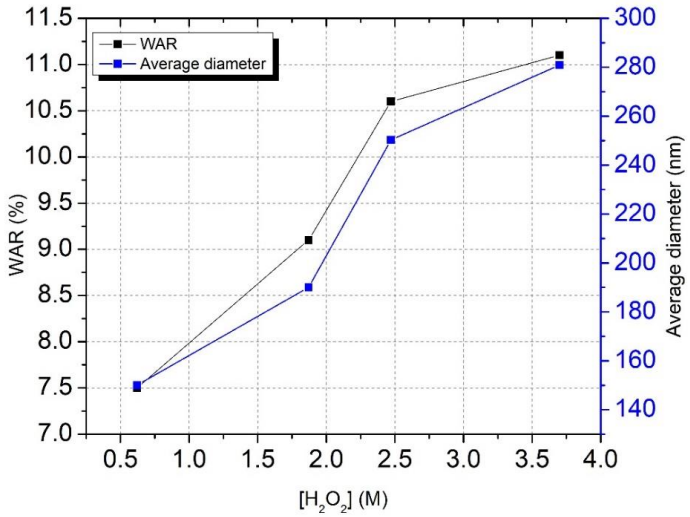

(b)

Figure 5: (a) Relationship between WAR and height of b-Si nanowires with different H_2O_2 concentrations (b) Relationship between WAR and average diameter of b-Si nanowires with different H_2O_2 concentrations.

From the result, it established that both the height and the mean average diameter of the nanowires are important in determining the WAR. While, the sizes of the base diameters are more important in determining the efficacy of the refractive index grading effect for lower WAR and an enhance optical absorption in the b-Si. The findings from this work correlate with Branz et. al. suggestions that nanowires with a mean grade depth of 250 nm are adequate to reduce the WAR to ~5.0% if the optimal nanowires' base diameter is achieved [29]. Besides, Chai et. al. recently reported that WAR increases with an increase in nanowires' diameter irrespective of the nanowires' length [30]. Therefore, further emphasis is given to understanding the effect of increased diameters of nanowires on the $J_{sc(max)}$ of the b-Si solar cells. Increased surface reflection defined by a high WAR, will always translate to lower $J_{sc(max)}$ of the b-Si solar cells. Thus, theoretical calculations using Eq.(2) are conducted

to further ascertains the effect of H_2O_2 concentrations (with emphasis on the effect of increased diameters) on potential $J_{sc(max)}$. This is presented in Table 2.

Table 2: Calculated potential $J_{sc(max)}$ and $J_{sc(max)}$ enhancement of b-Si wafers fabricated with different H_2O_2 concentrations (W: 0.62 M, X: 1.85 M, Y: 2.47 M and Z: 3.7 M). Potential $J_{sc(max)}$ of c-Si wafer is used as a reference.

H_2O_2 concentration (M)	**Potential $J_{sc(max)}$ (mA/cm^2)**	**Potential $J_{sc(max)}$ enhancement (%)**
Ref. c-Si	26.3	-
W: 0.62 M	38.2	45.2
X: 1.85 M	37.0	40.7
Y: 2.47 M	36.2	37.6
Z: 3.70 M	35.8	36.1

Table 2 presents the summarized results of potential $J_{sc(max)}$ and enhancement in $J_{sc(max)}$ for the W, X, Y, and Z b-Si samples produced with different concentrations of H_2O_2 (0.62 M, 1.85 M, 2.47 M, and 3.7 M). The $J_{sc(max)}$ of the un-etched c-Si is 26.3 mA/cm^2. Decreasing trend for the potential $J_{sc(max)}$ and enhancement in $J_{sc(max)}$ of the W, X, Y, and Z b-Si wafers is observed. This is due to continuous decrease in base diameters of the b-Si wafers produced for different concentrations of H_2O_2. With lower concentrations of H_2O_2 (0.62 M and 1.85 M; base diameters of 150 nm and 190 nm) the $J_{sc(max)}$ of the X b-Si sample (etched with 0.62 M concentration of H_2O_2) decreases to 37.0 mA/cm^2 from 38.2 mA/cm^2 of the W b-Si sample etched with 1.85 M concentration of H_2O_2. However, this still represent about 45.2% and 40.7% enhancements in the potential $J_{sc(max)}$ compared to $J_{sc(max)}$ of the un-etched reference planar c-Si. For samples Y and Z etched with high concentrations of H_2O_2 (2.47 M and 3.70 M) with average diameters of 250.3 and 280.9 nm, the $J_{sc(max)}$ of the b-Si wafers continuously decreases to 36.2 mA/cm^2 and 35.8 mA/cm^2. This represents only 36-38% of J_{sc} enhancement which is about 12.0% lower compared to when a low concentration of H_2O_2 (0.62 M and 1.85 M) with average diameters of 150 nm and 190 nm was employed during the b-Si fabrication. Overall, the superior enhancement in J_{sc} for b-Si fabricated with a low concentration of H_2O_2 owes to the formation of denser nanowires with precise average diameters (less than 200 nm). The denser nanowires helped to achieve the outstanding light-trapping in the b-Si. The achieved enhancement in J_{sc} is credited to the enhanced light absorption in the b-Si provided by the nanowires. The $J_{sc(max)}$ of both W, and X samples etched with 0.62 M and 1.85 M concentrations of H_2O_2 are nearly similar (38.2 mA/cm^2 and 37.0 mA/cm^2) even though the samples exhibit somewhat diverse length of nanowires and WAR that varied by about 1.6%. This shows that the WAR variation is not much to reflect in the $J_{sc(max)}$ calculation. Therefore, it is concluded that the difference in the length of nanowires does not much affect the $J_{sc(max)}$ compared to the sizes of the b-Si's average diameters.

Fig. 6 summarizes the relationship between H_2O_2 concentration, the average diameter of b-Si nanowires and $J_{sc(max)}$. Consistent with the results in Table 2, Fig. 6 shows that sample etched with 0.62 M concentration of H_2O_2 (sample W; with nanowires' heights of 900 nm and average diameter of 150 nm) presents the maximum achievable J_{sc} of 38.2 mA/cm^2 (or 45.2% enhancement compared to planar reference c-Si) due to possession of lowest WAR (7.5%) provided by the b-Si nanowires. The connection between Fig. 6 and developed nanowires typically rely on the indication that nanowires with precisely lower average diameters tend to produce

low WAR (i.e. 7.5 %, 9.1%, 10.6%, 11.1% for samples W, X, Y, and Z) and a high $J_{sc(max)}$ (i.e. 38.2 mA/cm^2, 37.0 mA/cm^2, 36.2 mA/cm^2, 35.8 mA/cm^2 for samples W, X, Y, and Z respectively). It is established that increased WAR provided by the higher average diameters of the b-Si nanowires causes the calculated $J_{sc(max)}$ to drop by ~12.0% compared to that of samples etched with low H_2O_2 concentrations.

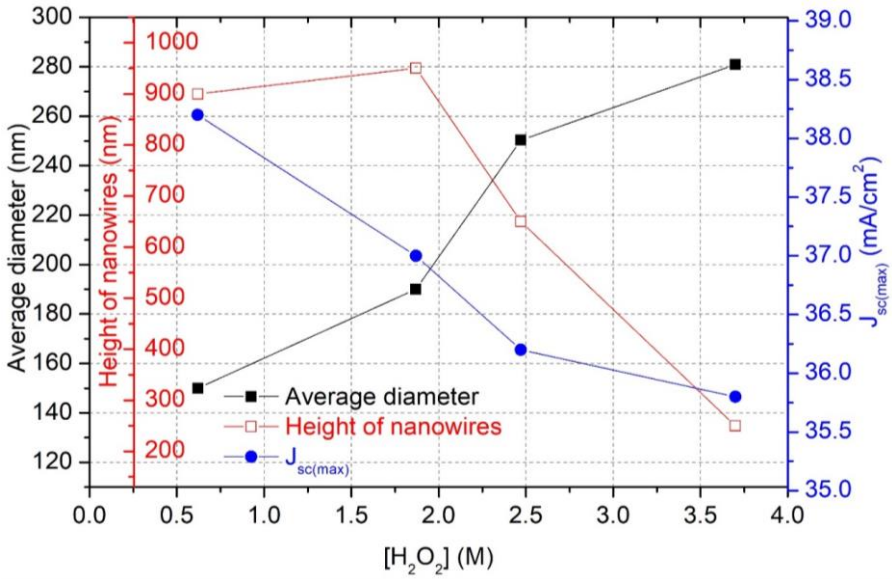

Figure 6: Relationship between average height, average diameter and $J_{sc(max)}$ of b-Si nanowires with different H_2O_2 concentrations.

4. Conclusion

In this work, the effect of H_2O_2 concentrations on broadband antireflection in b-Si produced via a two-step Ag-based MACE method has been studied. Low concentrations of H_2O_2 (0.62 M and 1.85 M) present b-Si samples (sample W and X) with nanowires' heights of 900-950 nm and precise average diameters of about 150-190 nm applicable for light-trapping applications. The nanowires suppress WAR to 7.5% and 9.1% with corresponding optical absorptions of up to 95.5% and 94.5% at a wavelength of 600 nm, respectively. Etching c-Si wafers with high concentrations of H_2O_2 (2.47 M and 3.70 M) presents b-Si samples (samples Y and Z) with nanowires' heights of 650 nm and 250 nm and enlarged average diameters of about 250.3 and 280.9 nm. This causes WAR to increase to 10.6% and 11.1%. For these samples, corresponding optical absorptions of only 93.4% and 92.2% at a wavelength of 600 nm, were obtained.

From this study, sample etched with 0.62 M concentration of H_2O_2 presents the maximum achievable J_{sc} of 38.2 mA/cm^2 (45.2% enhancement compared to planar un-etched c-Si) due to possession of lowest WAR (7.5%) provided by nanowires' average diameter of 150 nm. For higher concentrations of H_2O_2 (2.47 M and 3.70 M), the etching is slowed, and b-Si samples have nanowires with shorter average heights and enlarged average diameters which cause a decrease in the $J_{sc(max)}$ to ~36.0 mA/cm^2. Therefore, from this study, a low H_2O_2 concentration between 0.6-2.0 M is optimum for the realization of useful b-Si with nanowires having precise average diameters and high optical absorption applicable for light trapping applications in solar cells. However, for practical applications in b-Si solar cells, the challenge is to obtain a good electrical result as surface recombination of electrons and holes photogenerated charge carriers on nanotextured surfaces remain a critical issue. There

is always a trade-off between optical and electrical results. Addressing the challenge require an optimization and passivation of the interfaces between base and emitter layers of the b-Si solar cells using tunneling passivation oxides (e.g. SiO_2 and Al_2O_3) that already shows good perfect fit with c-Si and b-Si. Therefore, the focus is to develop efficient b-Si solar cells featuring SiO_2 and Al_2O_3 passivation for effective separation of electrons and holes charge carriers.

Acknowledgement

The authors would like to acknowledge Umaru Musa Yar'adua University Katsina, TetFund Nigeria and Universiti Sains Malaysia (USM) Penang, for supporting this research.

Conflict of interest

Authors declared that they have no conflict of interest.

References

1. *ITRPV, Trends and Challenges in c-Si PV - an update of the ITRPV 11 the edition (incl. maturity report).* 2021: pp. 1-3.
2. Battaglia C., Cuevas A., and De Wolf S., *High-efficiency crystalline silicon solar cells: status and perspectives.* Energy Environmental Science, 2016. **9**(5): pp. 1552-1576.
3. Zhuang Y., Zhong S., Huang Z., and Shen W., *Versatile strategies for improving the performance of diamond wire sawn mc-Si solar cells.* Solar Energy Materials Solar Cells, 2016. **153**: pp. 18-24.
4. Otto M., Algasinger M., Branz H., Gesemann B., Gimpel T., Füchsel K., Käsebier T., Kontermann S., Koynov S., and Li X., *Black silicon photovoltaics.* Black silicon photovoltaics, 2015. **3**(2): pp. 147-164.
5. Wang Y., Yang L., Liu Y., Mei Z., Chen W., Li J., Liang H., Kuznetsov A., and Xiaolong D., *Maskless inverted pyramid texturization of silicon.* Scientific reports, 2015. **5**(1): pp. 1-6.
6. Vazsonyi E., De Clercq K., Einhaus R., Van Kerschaver E., Said K., Poortmans J., Szlufcik J., and Nijs J., *Improved anisotropic etching process for industrial texturing of silicon solar cells.* Solar energy materials solar cells, 1999. **57**(2): pp. 179-188.
7. Da Y., Liu X., Xuan Y., and Li Q., *Photon management effects of hybrid nanostructures/microstructures for organic-silicon heterojunction solar cells.* International Journal of Energy Research 2018. **42**(15): pp. 4875-4890.
8. To W.-K., Tsang C.-H., Li H.-H., and Huang Z., *Fabrication of n-type mesoporous silicon nanowires by one-step etching.* Nano letters 2011. **11**(12): pp. 5252-5258.
9. Chen K., Zha J., Hu F., Ye X., Zou S., Vähänissi V., Pearce J.M., Savin H., and Su X., *MACE nano-texture process applicable for both single-and multi-crystalline diamond-wire sawn Si solar cells.* Solar Energy Materials Solar Cells, 2019. **191**: pp. 1-8.
10. Oh J., Yuan H.-C., and Branz H.M., *An 18.2%-efficient black-silicon solar cell achieved through control of carrier recombination in nanostructures.* Nature nanotechnology 2012. **7**(11): pp. 743-748.
11. Srivastava S.K., Kumar D., Sharma M., Kumar R., and Singh P., *Silver catalyzed nano-texturing of silicon surfaces for solar cell applications.* Solar Energy Materials Solar Cells, 2012. **100**: pp. 33-38.

12. Aca-López V., Quiroga-González E., Gómez-Barojas E., Światowska J., and Luna-López J.A., *Effects of the doping level in the production of silicon nanowalls by metal assisted chemical etching.* Materials Science in Semiconductor Processing 2020. **118**: pp. 1-15.
13. Abdulkadir A., bin Abdul Aziz A., and Pakhuruddin M.Z., *Optimization of etching time for broadband absorption enhancement in black silicon fabricated by one-step electroless silver-assisted wet chemical etching.* Optik 2019. **187**: pp. 74-80.
14. Li X., Gao Z., Zhang D., Tao K., Jia R., Jiang S., Wang B., Ji Z., Jin Z., and Liu X., *High-efficiency multi-crystalline black silicon solar cells achieved by additive assisted Ag-MACE.* Solar Energy Materials Solar Cells, 2020. **195**: pp. 176-184.
15. Behera A.K., Viswanath R., Lakshmanan C., Mathews T., and Kamruddin M., *Synthesis of silicon nanowalls exhibiting excellent antireflectivity and near super-hydrophobicity.* Nano-Structures Nano-Objects 2020. **21**: pp. 1-7.
16. Liu Y., Ji G., Wang J., Liang X., Zuo Z., and Shi Y., *Fabrication and photocatalytic properties of silicon nanowires by metal-assisted chemical etching: effect of H2O2 concentration.* Nanoscale research letters 2012. **7**(1): pp. 1-9.
17. Li S., Ma W., Chen X., Xie K., Li Y., He X., Yang X., and Lei Y., *Structure and antireflection properties of SiNWs arrays form mc-Si wafer through Ag-catalyzed chemical etching.* Applied Surface Science 2016. **369**: pp. 232-240.
18. Gonchar K.A., Moiseev D.V., Bozhev I.V., and Osminkina L.A., *Influence of H2O2 concentration on the structural and photoluminescent properties of porous silicon nanowires fabricated by metal-assisted chemical etching.* Materials Science in Semiconductor Processing, 2021. **125**: pp. 1-6.
19. Kern W., *The evolution of silicon wafer cleaning technology.* Journal of the Electrochemical Society 1990. **137**(6): pp. 1887-1892.
20. Noor N.A.M., Mohamad S.K., Hamil S.S., Devarajan M., and Pakhuruddin M.Z., *Effects of annealing temperature towards surface morphological and optical properties of black silicon fabricated by silver-assisted chemical etching.* Materials Science in Semiconductor Processing, 2019. **91**: pp. 167-173.
21. Abdulkadir A., Aziz A.A., and Pakhuruddin M.Z., *Impact of micro-texturization on hybrid micro/nano-textured surface for enhanced broadband light absorption in crystalline silicon for application in photovoltaics.* Materials Science in Semiconductor Processing, 2020. **105**: pp. 1-8.
22. Pakhuruddin M.Z., Dore J., Huang J., and Varlamov S., *Effects of front and rear texturing on absorption enhancement in laser-crystallized silicon thin-films on glass.* Japanese Journal of Applied Physics 2015. **54**(8S1): pp. 1-7.
23. Abouda-Lachiheb M., Nafie N., and Bouaicha M., *The dual role of silver during silicon etching in HF solution.* Nanoscale research letters, 2012. **7**(1): pp. 1-5.
24. Huang Z., Geyer N., Werner P., De Boor J., and Gösele U., *Metal-assisted chemical etching of silicon: a review: in memory of Prof. Ulrich Gösele.* Advanced materials 2011. **23**(2): pp. 285-308.
25. Chong T., Weber K., Booker K., and Blakers A., *Characterization of MAE-textured nanoporous silicon for solar cells application: Optics and surface passivation.* IEEE Journal of Photovoltaics 2014. **4**(5): pp. 1235-1242.

26. He X., Li S., Ma W., Ding Z., Yu J., Qin B., Yang J., Zou Y., and Qiu J., *A simple and low-cost chemical etching method for controllable fabrication of large-scale kinked silicon nanowires.* Materials Letters 2017. **196**: pp. 269-272.
27. Ma S., Liu S., Xu Q., Xu J., Lu R., Liu Y., and Zhong Z., *A theoretical study on the optical properties of black silicon.* AIP Advances 2018. **8**(3): pp. 1-8.
28. Plakhotnyuk M.M., Gaudig M., Davidsen R.S., Lindhard J.M., Hirsch J., Lausch D., Schmidt M.S., Stamate E., and Hansen O., *Low surface damage dry etched black silicon.* Journal of Applied Physics, 2017. **122**(14): pp. 1-9.
29. Branz H.M., Yost V.E., Ward S., Jones K.M., To B., and Stradins P., *Nanostructured black silicon and the optical reflectance of graded-density surfaces.* Applied Physics Letters, 2009. **94**(23): pp. 88-91.
30. Chai J.-H., Wong B.T., and Juodkazis S., *Black-silicon-assisted photovoltaic cells for better conversion efficiencies: a review on recent research and development efforts.* Materials Today Energy 2020. **18**: pp. 1-48.